RTO-MP-8
AC/323(AVT)TP/9

RTO-MP-8

NORTH ATLANTIC TREATY ORGANIZATION

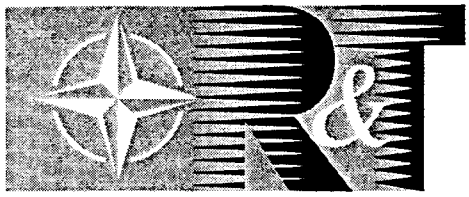

RESEARCH AND TECHNOLOGY ORGANIZATION
BP 25, 7 RUE ANCELLE, F-92201 NEUILLY-SUR-SEINE CEDEX, FRANCE

RTO MEETING PROCEEDINGS 8

Design Principles and Methods for Aircraft Gas Turbine Engines

(les Principes et méthodes de conception des turbomoteurs)

Papers presented at the RTO Applied Vehicle Technology Panel (AVT) Symposium - organized by the former AGARD Propulsion and Energetics Panel (PEP) - held in Toulouse, France, 11-15 May 1998.

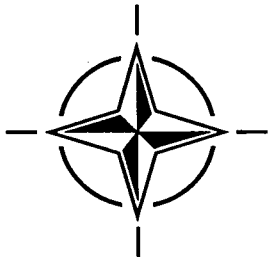

Published February 1999

AGARD - AVT Propulsion and Power Systems Symposium on Design Principles and Methods for Aircraft Gas Turbine Engines, Editor: G. Meauze, Toulouse, France, May 11-15, 1998.

Aero-Thermo-Structural Design Optimization of Internally Cooled Turbine Blades

G. S. Dulikravich[1], T. J. Martin[2], B.H. Dennis[2], E. Lee[2] and Z.-X. Han[3]
Department of Aerospace Engineering, 233 Hammond Bldg.
The Pennsylvania State University
University Park, PA 16802
U.S.A.

1. SUMMARY

A set of robust and computationally affordable inverse shape design and automatic constrained optimization tools have been developed for the improved performance of internally cooled gas turbine blades. The design methods are applicable to the aerodynamics, heat transfer, and thermoelasticity aspects of the turbine blade. Maximum use of the existing proven disciplinary analysis codes is possible with this design approach. Preliminary computational results demonstrate possibilities to design blades with minimized total pressure loss and maximized aerodynamic loading. At the same time, these blades are capable of sustaining significantly higher inlet hot gas temperatures while requiring remarkably lower coolant mass flow rates. These results suggest that it is possible to design internally cooled turbine blades that will cost less to manufacture, will have longer life span, and will perform as good, if not better than, film cooled turbine blades.

2. INTRODUCTION

The objective of this paper is to present several methods for the inverse design and optimization of the external and internal geometric shapes of internally cooled gas turbine blades. The design methods are pertinent to aerodynamics, heat transfer, and the structural integrity of the blades that can also have thermal barrier coatings. The ultimate goal is to sketch a multidisciplinary design procedure that is capable of maximizing inlet turbine temperature, and enhancing the uniformity of temperature and stress/deformation fields in the blade material, while at the same time minimizing coolant mass flow rate, inlet-to-exit total pressure loss, and coolant supply pressure. The methodologies discussed in this paper were chosen because they have been perceived to be the most robust and computationally affordable, while making minimal assumptions concerning the actual physics of the problem. Although most of the examples are two-dimensional, the methods are directly applicable to three-dimensional blade configurations. In order to demonstrate that a variety of the existing proven disciplinary analysis computer codes can be used in this design environment, we have intentionally used our finite difference, finite volume, finite element, and boundary element codes. They were written in different programming languages. Some of the codes were written for single structured grids, others for multi-block grids, and yet other codes were written for non-structured grids.

Similarly, our hybrid optimization software package utilizes several standard gradient-based and non-gradient optimization algorithms with a special logic for automatic switching among these modules in order to arrive at the global minimum. Each of the codes and design methodologies will be discussed briefly with the objective of conveying the essential design concept.

[1] Associate Professor.
[2] Graduate Research Assistant.
[3] Visiting Scholar.
Associate Professor, BUAA, Beijing, P. R. China.

There is a strong interaction among a number of engineering disciplines when studying the internally cooled gas turbine blades. We will consider aerodynamics of the hot gas flow in detail, coolant aerodynamics and heat transfer very approximately, heat conduction in the blade material very accurately, and stress/deformation field of the blade equally accurately. In the design process explained in this paper, these individual disciplines will not be solved simultaneously because this approach would take an unacceptably long time even on a cluster of workstations running in parallel. For these pragmatic reasons we opted for a computationally affordable sequential, loosely coupled, design approach as follows.

First, an initial realistic shape of a turbine blade was generated and the hot gas flow-field around it was analyzed using computational fluid dynamics (CFD). Then, if an aerodynamic performance improvement was desired, an inverse shape design of the blade was performed subject to the desired surface pressure distribution while accounting for fluid compressibility, heat transfer, and turbulence. If the aerodynamic performance was to be maximized, the blade shape was optimized subject to constraints such as fixed axial chord length, inlet and exit flow angles, minimum allowable trailing edge radius, and hot gas mass flow rate.

Next, the interior of the blade needed to be designed so that blade temperature was as uniform and as high as the blade material and life expectancy would allow. Since hot surface temperature specified in the external CFD analysis and aerodynamic shape design were arbitrary, these temperatures were modified by reshaping and resizing the interior coolant flow passages. This involved a certain amount of empiricism when dealing with the coolant flow-field and heat transfer, and it utilized optimization. The result was a new configuration of coolant flow passages that would allow for increased turbine inlet hot gas temperature and decreased coolant mass flow rate. At the same time, this optimized interior blade geometry matched the blade hot surface convection heat transfer coefficient distribution predicted by the CFD code and made the temperature field throughout blade as uniform as possible thus minimizing blade thermal stresses.

3. EXTERNAL AERODYNAMIC SHAPE INVERSE DESIGN AND OPTIMIZATION

Although only a few are suitable for fully three-dimensional turbine blade geometry design, a variety of aerodynamic shape inverse design methodologies exist in the open literature [Dulikravich, 1995]. The reason why the particular inverse shape design procedure used in this work was chosen was to reduce the overall computing time while taking into account viscosity, turbulence, heat transfer, and compressibility.

3.1 Aerodynamic Shape Inverse Design

First, an inviscid flow-field was predicted around an initial guess for the shape of an airfoil. A four stage Runge-Kutta structured

grid Euler solver was used with solid wall stationary boundary conditions on the airfoil surface until a combined average residual was reduced by four orders of magnitude, which was deemed to be an acceptably converged solution. An approximate factorized ADI algorithm was the basis of the steady-state solution of the Euler/Navier-Stokes code. A finite difference method on a block-structured non-orthogonal grid and explicitly added artificial dissipation terms were used in space discretization. Baldwin-Lomax turbulence modeling was used for turbulence closure in the Reynolds-averaged full Navier-Stokes solver.

Then, permeable wall boundary conditions were enforced causing a sudden increase in the combined average residual. The permeable wall boundary conditions are based on the signs of the eigenvalues of the Euler system of flow-field governing equations at the airfoil surface [Leonard; 1990; Leonard and Demeulenaere, 1997]. The permeable wall boundary conditions were enforced during every iteration with the Euler flow-field analysis code until the combined average residual decreased to the same level as it was when the initial flow-field was deemed converged (Fig. 1). At that moment, the airfoil normal surface coordinates were updated according to the geometry update formula.

$$\Delta n_{i-1}(\rho\tilde{W}_t)_{i-1} + \Delta s_i \frac{(\rho W_n)_i + (\rho W_n)_{i-1}}{2} = \Delta n_i(\rho\tilde{W}_t)_i$$

where

$$(\tilde{W}_t)_{i-1} = \left((W_t)_{i-1} + (W_t^{target})_{i-1}\right)/2$$

with a similar expression for $(\tilde{W}_t)_i$. Here, ρ is the local fluid density, W_n and W_t are the normal and tangential relative fluid velocity components at the airfoil surface, and Δn and Δs are the normal distance (local shape update value) and the local arc length of a surface grid cell, respectively. This transpiration concept (or quasi one-dimensional streamtube mass balance) equation was applied to the entire airfoil surface starting from the leading edge stagnation point. After the geometry update, the grid was regenerated in the domain near the airfoil and the flow-field variables were interpolated at the new grid points. This again caused a jump in the combined average residual. Euler equations with the characteristic surface boundary conditions were run again until the residual was reduced to the earlier level. At that moment, the geometry and the grid were updated again and the process continued. Usually, only 2-4 shape updates were needed (Fig. 1) with the Euler solver, depending on the magnitude of the geometry changes. The final surface pressure distribution almost duplicated the target surface pressure distribution.

The ultimate objective was to create the airfoil shape that was compatible with the actual viscous, turbulent flow with heat transfer. Therefore, the inverse shape design automatically proceeded by switching from the Euler mode to the full Navier-Stokes mode of the analysis code while enforcing solid wall boundary conditions on the shape just designed using the Euler solver. This step was necessary in order to develop boundary layer velocity profiles and possible flow separation regions before applying the final design step, which used the Navier-Stokes solver and impermeable moving wall boundary conditions [Leonard and Demeulenaere, 1997]. Here, the airfoil shape was updated and the new grid was generated during each iteration with the Navier-Stokes code. In this method, it was beneficial to keep the grid velocity term in the contravariant velocity components defined as

$$U = \frac{D\xi}{Dt} = \frac{\partial\xi}{\partial t} + u\frac{\partial\xi}{\partial x} + v\frac{\partial\xi}{\partial y}$$

$$V = \frac{D\eta}{Dt} = \frac{\partial\eta}{\partial t} + u\frac{\partial\eta}{\partial x} + v\frac{\partial\eta}{\partial y}.$$

The grid velocity term was calculated by following a space conservation law [Demirdzic and Peric, 1988]

$$\frac{\partial}{\partial t}\left(\frac{1}{J}\right) + \frac{\partial}{\partial\xi}\left(\frac{\partial\xi}{\partial t}\right) + \frac{\partial}{\partial\eta}\left(\frac{\partial\eta}{\partial t}\right) = 0$$

where J is the local Jacobian of the geometric transformation from the Cartesian x,y coordinates to the non-orthogonal curvilinear boundary conforming coordinates, ξ, η. The airfoil geometry was updated at every iteration by the same surface transpiration formula as in the case of the inviscid design, except that now $W_n = W_t = 0$ on the airfoil surface [Leonard, 1990].

The first example using this inverse shape design approach illustrated the redesign of a cascade of non-staggered NACA0012 airfoils at zero angle of attack with gap/chord ratio g/c = 2.0. The flow conditions were: Po1 = 286356 Pa, To1 = 1600 K, Pexit = 234910 Pa, dynamic viscosity $\mu = 5\text{x}10^{-5}$ kg m^{-1} s^{-1}, specific gas constant R = 210 J kg^{-1} K^{-1}, ratio of specific heats γ = 1.4, reference length L = 0.1 m. This resulted in Prandtl number Pr = 0.72 and Reynolds number Re = 1 x 10^6 where the reference speed was the inlet stagnation speed of sound. The corresponding inlet Mach number was M = 0.5. Airfoil surface was treated as adiabatic. A single C-type grid was used with 193 x 33 = 6569 grid points. A target surface pressure distribution higher than the initial surface pressure distribution was imposed. Figure 2 indicates that the converged pressure distribution was in good agreement with the target pressure distribution and the final geometry was thicker than the initial airfoil. The flow-field was separated on the initial geometry starting from 80% of the chord (Fig. 3) while the final geometry had considerably smaller flow separation, which started at 96% of the chord (Fig. 4), because the transpiration method updated the geometry based on a streamtube approach. The convergence history of this iterative process (Fig. 1) depicts the first 1200 iterations performed with the inviscid version of the code while using permeable wall boundary conditions. During these 1200 iterations with the Euler solver, the airfoil geometry was updated three times (after 400, 800, and 1200 iterations). The Navier-Stokes solver with no-slip boundary conditions was then activated for 50 iterations to develop boundary layer velocity profiles. Finally, this was followed by the application of the Navier-Stokes code using a moving solid boundary formulation, that is, updating the airfoil shape and the grid after each iteration. This calculation was performed on an SGI Solid Impact R10000 workstation with a 175MHz processor and took 11 minutes, which was about 3.5 times as much computing time as required for one flow-field analysis with the Navier-Stokes code.

The second example involved the inverse shape design of a turbine cascade with high subsonic exit flow. The flow conditions were: Po1 = 600000 Pa, To1 = 1600 K, dynamic viscosity $\mu = 8\text{x}10^{-5}$ kg m^{-1} s^{-1}, specific gas constant R = 210 J kg^{-1} K^{-1}, ratio of specific heats γ = 1.3, reference length L = 0.08 m. This resulted in Prandtl number Pr = 0.72 and Reynolds number Re = 1.18 x 10^6 where the reference speed was the inlet stagnation speed of sound. Exit static pressure, Pexit = 367420 Pa, was enforced thus making the exit isentropic Mach number M = 0.87. Temperature equal to 75% of To1 was enforced on the airfoil external surface. For better accuracy, an O-H-C multi-block grid was used where the total number of grid points was 11900. Figure 5 shows the initial, target, and final computed isentropic Mach number distributions on the airfoil surface versus airfoil contour arc length and the initial and final airfoil shapes. The Mach number distribution on the new

turbine airfoil was smoother in the nose and suction regions, and the Mach number dip on the pressure surface disappeared. Initial and final pressure contour lines are displayed in Figs. 6 and 7. This shape design consumed almost 3 hours of CPU time on the SGI workstation because this test case converged slower than the previous non-lifting case.

The same shape inverse design procedure was also implemented in a fully three-dimensional version of our Navier-Stokes analysis code using either a single C-type grid or a three-dimensional block-structured O-C-H grid. An inverse shape design required typically five times as much computing time as a single flow-field analysis.

3.2 Aerodynamic Shape Optimization of a Supersonic Exit Cascade

When a global objective is to be reached (for example, minimum total pressure loss from inlet to exit of a turbine cascade), the flow-fields for a large number of cascade shapes must be analyzed. Since geometric variations explored may not be small, it is of utmost importance that a robust grid generation code and a robust CFD code are used. For this reason a robust compressible turbulent flow Navier-Stokes analysis code was used that utilized non-structured triangular grids [Han and Liu, 1997; Han et al., 1998]. The blade airfoil geometry was generated using eight parameters [Dennis and Dulikravich, 1997] that became design variables in the shape optimization process. The non-structured grid was generated using an advancing front method [Pirzadeh, 1993]. All boundary conditions in the flow solver were imposed using first order accuracy. The inlet and outlet boundary conditions were treated with locally 1-D non-reflection of waves passing out of the computational domain. Implementation of the 2-D non-reflection boundary conditions at inlet and exit boundaries would take many more operations than 1-D non-reflection boundary conditions. Periodic flow conditions were imposed with the phantom cells' values equal to the corresponding periodic real cells' values. The flow variables at the cells' vertices were calculated from surrounding cells centers' values with the distance weighted averaging method. The k-ε limiter and wall function were used in turbulence modeling.

As an example of the robust constrained aerodynamic shape optimization, the same cascade of turbine airfoils with a supersonic average exit Mach number M = 1.4 was created by lowering the exit static pressure to 101330 Pa (Fig. 9). By varying randomly the eight design variables (conic sections) controlling the airfoil shape, a population of 30 initial airfoil cascades was formed. The design objective was: maximize lift, minimize total pressure loss, enforce an exit angle between -58 and -62 degrees. At the same time, axial chord and airfoil-to-airfoil vertical distance (gap) were kept fixed.

Using a constrained genetic algorithm and the non-structured turbulent compressible flow Navier-Stokes solver, the entropy field and the Mach number field for the best cascade in the initial population of 30 cascades are depicted in Fig. 8. After 10 generations, that is, after generating the shapes and analyzing the flow-fields of 10 x 30 = 300 cascades, the best turbine airfoil cascade evolved to a significantly different shape (Fig. 9) having only half the original entropy rise and much weaker shocks. The stagger angle was not constrained and it increased significantly (Fig. 10). Airfoil thickness was also unconstrained resulting in a very thin airfoil that would be unacceptable for reasons of structural integrity and cooling passage manufacturability. The trailing edge radius converged to the minimum allowable value (as expected) (Fig. 10). The best design had an exit angle of -60.5 which is almost on the constraint boundary (it should converge to -60.0) (Fig. 11).

4. THERMAL SHAPE OPTIMIZATION

4.1 Interior Geometry Generation

The first step in the design of the multiple coolant flow passages was the description of the cooling wall thickness function; W(s), which determined the thickness of the wall between the hot gas and the coolant fluid. The abscissa, s, followed counter-clockwise along the metal/coating interface all the way around the airfoil, from trailing edge to trailing edge and formed a closed loop. W(s) was described by a piecewise-continuous β-spline curve that varied in the direction normal to the metal/coating interface to a distance controlled by one design variable per β-spline control vertex. One or more thermal barrier coatings with a specified thickness was added by generating additional congruent airfoil shapes inward to the outer airfoil surface. The coating thickness distribution was described using the β-splines so that it varied from point to point along the airfoil contour, allowing for greater thermal barrier protection in areas which were hotter, but thin in other areas that were more sensitive to spalation problems.

The x-coordinates of the intersections of the struts' centerlines with the outer turbine airfoil contour were defined as x_{Ssi} and x_{Spi}, for the suction and pressure sides, respectively. Figure 12 illustrates the complete geometric modeling of the coolant flow passages and thermal barrier coating. The range over which each strut could vary was specified and the number of coolant flow passages in the turbine airfoil was specified. Since the number of coolant passages may also be a design variable, a problem would arise when computing the gradient of the objective function in a typical gradient-based optimization algorithm. Additional coolant passages could not easily be added since the searching capabilities of the optimizer could never include all the possible combinations of passage locations and geometry. Therefore, a simple and straightforward approach was utilized by starting the optimization with a large number of passages (limited only by available computer memory and computer speed) and then automatically reducing the number of passages during the optimization procedure [Dulikravich and Kosovic, 1992; Dulikravich and Martin, 1994; Dulikravich, 1988]. Any particular coolant passage was eliminated whenever it was reduced to such a small size that it had a negligible effect on the heat flux at the hot outer boundary of the airfoil. In addition to the end-coordinates of the struts, the strut thickness, t_{Si}, and a filleting Lame curve exponents on the pressure and suction sides, e_{Sti} and e_{Sli}, respectively, were used to complete the geometric modeling of each strut (Fig. 12). The three-dimensional turbine blade was then generated by stacking the two-dimensional sections including a twist about the stacking axis, scaling of the sectional shapes, and yawing of the stacking axis.

4.2 A Model for Quasi-Conjugate Heat Transfer

It would be highly desirable, and it is theoretically feasible, to construct a conjugate heat transfer analysis [Li and Kassab, 1994] that simultaneously solves the fully three-dimensional turbulent compressible hot gas flow-field, the heat conduction within the turbine blade material, and the fully three-dimensional turbulent compressible coolant flow-field. At present, the computational time needed for this type of analysis is still too long for numerical optimization purposes. Therefore, a simpler semi-conjugate heat transfer analysis and optimization of the turbine blade was developed with the objective of avoiding extremely complex, computationally demanding, and unreliable task of repetitively predicting the fully three-dimensional turbulent compressible coolant flow-field [Stephens and Shih, 1997]. Specifically, the application of thermal boundary conditions on the coolant flow passage walls was greatly simplified by the specification of convective heat transfer coefficients and ambient fluid temperatures of the coolant fluid.

$$q'' = -k_M \frac{\partial T}{\partial n} = h_{cool,n}\left(T_w - T_{cool,n}\right)$$

Here, k_M is the coefficient of thermal conductivity of the metal blade. The convective heat transfer coefficient, h_{cool}, on the walls of the nth coolant passage was allowed to vary with the following parameters: velocity of the coolant, V_{cool}, coolant density, ρ_{cool}, the hydraulic diameter, D_h, temperature of the passage wall, T_w, bulk temperature of the coolant, T_{cool}, average wall roughness height, ε, temperature-dependency of the fluid properties, μ_{cool}, k_{cool}, c_{pcool}, thermal buoyancy, $g\beta$, and the geometric shape of the coolant passage. This list of 11 variables was replaced by 7 non-dimensional variables which were all based upon the bulk coolant flow properties [White, 1988, Chapter 5].

$$S_t = f\left(Re_D, Pr, \frac{\varepsilon}{D_h}, \frac{T_w}{T_{cool}}, Gr_D, Ec, shape\right)$$

where the non-dimensional numbers are:

Stanton number $St = \dfrac{h_{cool}}{\rho_{cool} c_{p_{cool}} V_{cool}}$,

Reynolds number $Re_D = \dfrac{\rho_{cool} V_{cool} D_h}{\mu_{cool}}$,

Prandtl number $Pr = \dfrac{\mu_{cool} c_{p_{cool}}}{k_{cool}}$,

Grashof number $Gr_D = \dfrac{g\beta\left(T_w - T_{cool}\right) {D_h}^3}{\left(\mu_{cool}/\rho_{cool}\right)^2}$,

Eckert number $Ec = \dfrac{V_{cool}^2}{c_{Pcool}\left(T_w - T_{cool}\right)}$,

Nusselt number $Nu_D = \dfrac{h_{cool} D_h}{k_{cool}}$, and

friction factor, $f = \dfrac{8\tau_w}{\rho_{cool} {V_{cool}}^2}$.

The following assumptions were made in order to simplify these correlations and to arrive at a usable functional relationship. The temperature differences in the coolant were assumed to be small enough to eliminate temperature-dependent physical properties. Thermal buoyancy and viscous dissipation effects were neglected as were the centripetal and Coriolis acceleration effects. Results of experimental data for this type of simplified forced convection heat transfer are quite common in the open literature. Correlations for rough surface tubes, such as those containing trip strips, are rather sparse. The Reynolds analogy is often used to produce a solution under these circumstances.

$$St\, Pr^{0.667} = \frac{f}{8}$$

The friction factor, f, was related to the pressure loss in the coolant passage by the well-known formula for fully developed pipe flows driven only by the pressure gradient

$$\Delta p = f \frac{L}{D} \rho_{cool} \frac{{V_{cool}}^2}{2}.$$

The value of the local friction factor could be taken from the Moody chart knowing the relative surface roughness, ε/D, of the particular section of the coolant passage and the corresponding local Reynolds number [Holman, 1981, p. 230]. For optimization purposes, the friction factor should be allowed to change during the optimization process. Therefore, an explicit formula given by Haaland was used [White, 1994, p. 317] where maximum allowable relative roughness can be specified.

$$\frac{1}{f^{1/2}} = -1.8 \log_e \left[\frac{6.9}{Re_D} + \left(\frac{\varepsilon/D}{3.7} \right)^{1.11} \right]$$

This explicit expression is accurate to within 2% of the Moody chart, which itself is accurate to +/-15% versus experimental data for fully turbulent flows having Reynolds numbers in the range $10^3 < Re < 10^8$. During the numerical optimization procedure, the relative wall roughness in the turbulent flow coolant passage was a design variable [White, 1994] that was allowed to increase up to $\varepsilon/D = 0.15$. Large relative wall roughness values simulated the effect of placing pin fins and trip strips on the coolant passage walls. Because the coolant passages do not, in general, have a circular cross section, these heat transfer correlations were based on the local hydraulic diameters of the coolant passages, $D_h = 4A_h/P_h$, where A_h is the cross-sectional area and P_h is the wetted perimeter. Given the coolant mass flow rate, $\dot{m} = \rho_{cool} A_h V_{cool}$, the local average velocity of the coolant and the corresponding local Reynolds numbers were computed.

The coolant mass flow rate was allowed to vary during the optimization process so that it could be correlated with the limiting temperature on the hot surface of the turbine blade. Only the inlet coolant fluid temperature was specified and kept fixed.

The coolant streamwise pressure gradients were calculated for each coolant passage section given the empirical relationships previously described, $dp/dz = \Delta p/L$. These pressure gradients were used to determine the minimum required coolant supply pressure. That is, the static pressure, p_{cool}, at the inlet of the first coolant flow passage (at the root of the blade leading edge) was determined given the pressure losses in the entire coolant passage and the knowledge of a fixed static pressure, p_{static}, at the exit of the last coolant flow passage segment (assumed to be equal to the hot gas pressure at the blade trailing edge). Because the relationship between the coolant pressure loss and coolant inlet pressure was implicit, the bisection method was used to determine the root of the following function.

$$p_{eject}\left(\dot{m}, \varepsilon/D, p_{cool}\right) - p_{static} = 0$$

In this equation, the ejection static pressure, p_{eject}, was calculated given an initial guess to p_{cool} and the computed pressure losses, Δp. It was a function of the coolant mass flow rate, the coolant passage wall relative roughness, the inlet coolant pressure, as well as the blade and coating material properties and coolant passage geometry. In the case of trailing edge coolant ejection, the exit coolant static pressure, p_{static}, could be computed by a CFD prediction of the external hot flow through the turbine cascade. In the case of a closed loop cooling systems, p_{static} can be specified from an experimental evaluation.

The ambient (bulk) coolant temperatures in each of the coolant passages were allowed to be a non-linear function of heat flux, $T_{cool} = T_{cool}(Q)$. A quasi one-dimensional, steady state, incompressible, thermal energy equation was used to determine the bulk coolant temperatures and pressures along the entire length of the serpentine coolant flow passage.

$$\int \dot{m} c_p \frac{dT_{cool}}{dz} dz = \iint Q ds dz + \int \frac{\dot{m}}{\rho_{cool}} \frac{\Delta p}{T_N} dz$$

Here, Q is the heat flux through the coolant passage walls, s is the contour-following variable along the coolant wall perimeter,

and z is the coolant streamwise direction. This equation was written for each coolant passage including 180 degree turn sections and solved for the local streamwise temperature gradients, $(dT_{cool}/dz)_N$. For this purpose, we used blade outer hot surface temperatures and heat fluxes that were previously computed by the CFD analysis of the hot gas flow-field with blade wall temperatures guessed as 75% of the cascade inlet hot gas temperature. Because T_{cool} is a function of Q, the solution of the heat conduction equation in the blade material was non-linear due to the heat flux dependent ambient coolant temperature [Chyu et al., 1997] in the convection heat transfer boundary conditions. Subsequent solutions to the heat conduction provided better estimates of the heat flux, Q, and the iterative scheme proceeded until the computed heat fluxes converged. This was typically accomplished in a maximum of five solutions of the heat conduction problem in the entire airfoil.

This simplified approach to conjugate heat transfer did not fully account for all of the heat transfer characteristics in real rotating serpentine coolant flow passages which are very complex and three-dimensional, being affected by Coriolis and centripetal forces combined with thermal buoyancy [Han et al., 1994; Moshizuki et al., 1994]. Further study is needed in these areas before an empirical correlation between the heat transfer rate and rotation can be reliable within the ranges of Reynolds, Grashof, and rotation numbers encountered in a real turbine blade.

Thus, our present approach should be understood as an effective combination of the presently available experimentally obtained correlations combined with detailed computations of the hot gas flow-field and the heat conduction in the blade material with the ultimate goal of providing a computationally affordable preliminary optimization tool. This design tool should iteratively arrive at the optimized coolant flow passage geometry inside a cooled turbine blade so that coolant mass flow rate is reduced while increasing the hot gas inlet temperature and making the temperature field in the blade material as uniform as possible.

4.3 Heat Conduction Analysis

The mathematical model for steady heat conduction within an internally cooled turbine blade was represented by a boundary value problem over a multiply-connected domain resulting in a steady-state, nonlinear heat conduction equation. This equation was numerically integrated with the Boundary Element Method (BEM) because of its advantages over finite element and finite difference methods since the BEM did not require grid generation in the domain [Brebbia and Dominguez, 1989]. In addition, the BEM was found to be faster and more accurate than the other methods for this type of boundary value problems especially when very thin thermal barrier coatings were present.

4.4 Thermal Shape Optimization

The thermal design engineer does not know in advance the temperature and heat flux distributions on the external turbine blade surface. In order to develop the most effective thermal shape optimization strategy, three different thermal objective functions have been studied [Martin and Dulikravich, 1997]. It was observed that an objective function, F(Vi), based on integrated temperature difference was the most appropriate choice.

$$F(V_i) = \left\{ \int_\Gamma (T - \overline{T})^2 \, d\Gamma \right\}$$

where Γ is the outer boundary of the blade. Here, the user specifies the desired average temperature, $\overline{T}$, within the material of the turbine blade. This temperature should be as high as possible while taking into account thermal creep and thermal cycle fatigue limitations of the blade material. The numerical optimization algorithm modified the geometry of the coolant passages in order to minimize the sum of squared differences between the local computed temperatures and the desired uniform temperature for each of the geometric perturbations. As this function was minimized, the temperature field within the turbine blade approached the desired value, $\overline{T}$, while reducing the temperature gradients and producing a more uniform temperature field.

4.5 Implicit Differentiation for Thermal Design Sensitivity Coefficients

The partial derivatives of the field variables (temperatures, temperature gradients, thermal conductivity, etc.) and boundary values (heat fluxes, heat transfer coefficients, etc.) with respect to a set of parameters, Vi, called design variables, are very useful when performing a parametric study of a particular design. These partial derivatives are called design sensitivity coefficients. The implementation of gradient-based numerical optimization algorithms for inverse thermal shape design and optimization require these partial derivatives as part of their operation. In general, there are four methods that can be used to determine sensitivity coefficients: 1) analytical differentiation, 2) numerical differentiation of the solution by finite differences, 3) direct implicit differentiation of the governing equations, and 4) the adjoint variable or control theory method. In the arena of modern applied numerical methods and computational fluid dynamics, analytic differentiation of the governing equations is still unreliable while the adjoint variable method requires a very complicated formulation of the optimization problem that needs to be developed uniquely for each objective function. Finite differencing, although the most common brute force method, is also the most expensive strategy of obtaining sensitivity coefficients. For example, if second-order central differencing is used, the governing system must be evaluated twice per every design variable per every optimization cycle iteration. When using the BEM, the implicit differentiation of the equations at the system level [Meric, 1995] offers a practical design sensitivity calculation because the factorization of coefficient matrices needs to be performed only once and stored. Kane and Saigal [1988] obtained the sensitivity coefficients by the implicit differentiation of the coefficient matrices formed by the boundary integral equations of two-dimensional sub-structural problems. This method has been extended to three-dimensional elasticity problems by Yamazaki et al. [1994]. Similarly, the system of boundary integral equations governing heat transfer in the blade material was differentiated with respect to the vector of design variables, V_i.

$$\frac{\partial c(x)}{\partial V_i} T(x) + c(x) \frac{\partial T(x)}{\partial V_i} + \int_{-1}^{1} \frac{\partial q^*(x,\xi)}{\partial V_i} T(\xi) |\vec{\eta}| \, d\xi$$

$$+ \int_{-1}^{1} q^*(x,\xi) \frac{\partial T(\xi)}{\partial V_i} |\vec{\eta}| \, d\xi + \int_{-1}^{1} q^*(x,\xi) T(\xi) \frac{\partial |\vec{\eta}|}{\partial V_i} d\xi$$

$$= \int_{-1}^{1} \frac{\partial u^*(x,\xi)}{\partial V_i} q(\xi) |\vec{\eta}| \, d\xi + \int_{-1}^{1} u^*(x,\xi) \frac{\partial q(\xi)}{\partial V_i} |\vec{\eta}| \, d\xi$$

$$+ \int_{-1}^{1} u^*(x,\xi) q(\xi) \frac{\partial |\vec{\eta}|}{\partial V_i} d\xi$$

The derivatives of the boundary conditions were found in the same way.

Dirichlet $\overline{\frac{\partial T}{\partial V_i}} = 0$ Neumann $\overline{\frac{\partial q}{\partial V_i}} = 0$

Robin
$$-k\frac{\partial q}{\partial V_i} - \frac{\partial k(T)}{\partial T}\frac{\partial T}{\partial V_i}q = \frac{\partial h_{conv}}{\partial V_i}(T - T_{amb}) + h_{conv}\left(\frac{\partial T}{\partial V_i} - \frac{\partial T_{amb}}{\partial V_i}\right)$$

After discretization, but before the application of boundary conditions, the linear algebraic system can be expressed in the following form.

$$[C']\{T\} + [C]\{T'\} + [H']\{T\} + [H]\{T'\} = [G']\{Q\} + [G]\{Q'\}$$

Here, the apostrophe denotes differentiation with respect to the design variables. In our present research, implicit differentiation of the fundamental solution has been avoided by using a slightly more expensive method of finite differencing of the coefficient matrices [C'], [H'], and [G']. Thus, the equation used was

$$[H'] = \frac{[H(V_i + \Delta V_i)] - [H(V_i)]}{\Delta V_i}$$

Using this equation, the boundary needs to be integrated once for every design variable perturbation. The advantage of this approach over implicit differentiation of the fundamental solution is that it was very easy to program; particularly because it did not require the implementation of hyper-singular integration. Since most computing time is involved in the factorization of the coefficient matrix [A],

$$[A]^{-1}\left\{\frac{\partial X}{\partial V_i}\right\} = -[C']\{T\} - [H']\{T\} + [G']\{Q\} + \left\{\frac{\partial F}{\partial V_i}\right\}$$

rather than during the integration over the boundary, this method still provided a substantial reduction in computational time at the expense of the memory required to store two sets of BEM coefficient matrices. The linear system of equations was then solved for the unknown derivatives of temperature and flux $\partial T/\partial V_i$ and $\partial q/\partial V_i$. The gradient of the thermal objective function, as well as its design sensitivity, has been computed given the thermal sensitivity coefficients of $\partial T/\partial V_i$.

$$F(V_i) = \int_\Gamma 2(T - \overline{T})\frac{\partial T}{\partial V_i}d\Gamma$$

It should be pointed out that instead of using a thermal penalty function, the thermal constraint, $T_{max} = \overline{T}_{max}$, was placed directly into design sensitivity.

4.6 Evolutionary Hybrid Optimization

Since the design space for typical non-linear large-scale multidisciplinary optimization problems had an abundance of local minimums, it was advantageous to use a constrained evolutionary hybrid optimization approach [Foster and Dulikravich, 1997; Martin and Dulikravich, 1997] in order to avoid local minimums. The hybrid algorithm incorporated four of the most popular optimization approaches: the Davidon-Fletcher-Powell (DFP) gradient search method, a genetic algorithm (GA), the Nelder-Mead (NM) simplex method, and simulated annealing (SA). Each technique separately provided a unique approach to optimization with varying degrees of convergence, reliability, and robustness at different stages during an iterative optimization procedure. The new evolutionary hybrid scheme treated the existence of constraints in three ways: Rosen's projection method, a feasible search, and random design generation. Rosen's projection method [Haftka and Gurdal, 1992] provided search directions which guided the descent direction tangent towards active constraint boundaries. In the feasible search, designs that violated constraints were automatically restored to feasibility via the minimization of the active global constraint functions. If at any time this constraint minimization failed, a number of random designs were generated using a Gaussian-shaped probability density cloud about a desirable and feasible design until a new design was reached.

The feasible set of design variables from the current optimization cycle was saved into an array called the population matrix. This population was updated every iteration with new designs which were ranked according to the value of the objective function so that as the optimization process proceeded, the population evolved. The optimization problem was completed when the best design in the population was equivalent to a target design or when every optimizer failed to arrive at a better design simultaneously. This usually indicated that a global minimum had been found.

4.7 Results of Quasi-Conjugate Thermal Optimization

An example of the potential practical benefits of using this approach to design optimization of coolant flow passages based on the quasi-conjugate heat transfer optimization is demonstrated in Figs. 13-20. A symmetric Rankine oval shape (Fig. 13) was chosen to simulate a typical support strut airfoil. It was modeled as being made of stainless steel with thermal conductivity k = 30.0 W m^{-1} K^{-1} and having a 150 microns thick thermal barrier coating with thermal conductivity, k = 1.0 W m^{-1} K^{-1}. The strut airfoil was assumed to have four coolant flow passages that were initially symmetrically sized and located (Fig. 13). For specified temperatures (Fig. 14) on the outside surface of the strut airfoil, the structured grid Navier-Stokes code predicted the corresponding surface normal temperature derivatives from which the heat convection coefficient distribution (Fig. 15) was obtained using inlet hot gas temperature as the ambient temperature. The desired average temperature in the entire airfoil was specified to be $\overline{T}$ = 1300 K. There were 20 geometric design variables in this test case: 8 vertices of the b-spline for the blade wall thickness, 2 strut x-locations/strut, 1 strut thickness/strut, and 1 filleting parameter (Lame curve exponent)/strut. Using this flexible geometry treatment of the interior of the airfoil and using the quasi conjugate heat transfer optimization, the four coolant flow passages converged to their new shapes and locations (Fig. 13). The corresponding temperature distribution on the airfoil outer surface was more uniform than the initial surface temperature distribution. Even the leading edge stagnation point temperature was decreased slightly (Fig. 14). At the same time, the optimized coolant passages allowed for a significantly higher inlet hot gas temperature (Fig. 16) and a considerably lower coolant mass flow rate (Fig. 17) which is a remarkable result. Notice also that the final result was symmetric about x-axis. Coolant pressure loss increased (Fig. 18) during the quasi-conjugate optimization because of the increased optimized relative surface roughness (Fig. 19) required on the walls of each of the coolant passages. This in turn lead to the increased average convection heat transfer coefficient (Fig. 20) on the walls of each of the coolant passages. The entire design optimization process required two hours of a single processor time on Cray C-90 computer.

5. THERMOELASTICITY

Several methods have been developed for inverse determination of deformations and tractions on boundaries of solids (Figs. 21-23) where these quantities cannot be readily obtained because of inaccessibility or a hostile environment. Recently, a very accurate method based on finite elements has been developed [Dennis and Dulikravich, 1998] capable of simultaneously determining surface deformations and tractions.

6. SUMMARY

A number of methods for inverse shape design and optimization in the field of aerodynamics and heat transfer have been exposed with an objective of illustrating possibilities for an automated multidisciplinary design environment that can offer significant improvements in the efficiency of the new generation of high temperature internally cooled turbomachinery blades.

7. ACKNOWLEDGMENTS

The authors are grateful for NASA-Penn State Space Propulsion Engineering Center Graduate Student Fellowship, National Science Foundation Grant DMI-9522854 monitored by Dr. George Hazelrigg, NASA Lewis Research Center Grant NAG3-1995 facilitated by Dr. John Lytle, and supervised by Dr. Kestutis Civinskas, and the ALCOA Foundation Faculty Research Fellowship facilitated by Dr. Yimin Ruan.

8. REFERENCES

Brebbia, C. A. and Dominguez, J. (19890 *Boundary Elements, An Introductory Course,* McGraw-Hill Book Company, New York.

Chyu, M. K., Ding, H., Downs, J. P., Van Sutendael, A. and Soechting, F. O. (June 1997) "Determination of Local Heat Transfer Coefficient Based on Bulk Mean Temperature Using a Transient Liquid Crystals Technique", ASME paper 97-GT-489, Orlando, FL.

Demirdzic, I. and Peric, M. (1988) "Space Conservation Law in Finite Volume Calculations of Fluid Flow ", *International J. for Numerical Methods in Fluids*, Vol. 8, pp. 1037-1050.

Dennis, B. H. and Dulikravich, G. S. (September 1997) "Thermo-Elastic Analysis and Optimization Environment for Internally Cooled Turbine Airfoils", Symp. on Airbreathing Engines, Ed: F. S. Billig, Chattanooga, TN, Sept. 8-12, 1997, ISABE 97-7181, Vol. 2, pp. 1335-1341.

Dennis, B. H. and Dulikravich, G. S. (March 1988) "A Finite Element Formulation for the Detection of Boundary Conditions in Elasticity and Heat Transfer", *International Symposium on Inverse Problems in Engineering Mechanics – ISIP'98*, Editor: M. Tanaka, Nagano City, Japan, March 24-27, 1998.

Dulikravich, G. S. (June 1988) "Inverse Design and Active Control Concepts in Strong Unsteady Heat Conduction", *Appl. Mechanics Reviews*, Vol. 41, No. 6, pp. 270-277.

Dulikravich, G. S. (January 1995) "Shape Inverse Design and Optimization for Three-dimensional Aerodynamics", *AIAA Invited Paper 95-0695*, AIAA Aerospace Sci. Meet., Reno, NV.

Dulikravich, G. S. and Kosovic, B. (1992) "Minimization of the Number of Cooling Holes in Internally Cooled Turbine Blades", *International Journal of Turbo & Jet Engines*, Vol. 9, No. 4, pp. 277-283.

Dulikravich, G. S. and Martin, T. J. (1994) "Inverse Design of Super-Elliptic Cooling Passages in Coated Turbine Blade Airfoils", *AIAA Journal of Thermophysics and Heat Transfer*, Vol. 8, No. 2, pp. 288-294.

Dulikravich, G. S. and Martin, T. J. (1995) "Geometrical Inverse Problems in Three-Dimensional Non-Linear Steady Heat Conduction", *Engineering Analysis with Boundary Elements*, Vol. 15, pp. 161-169.

Dulikravich, G. S. and Martin, T. J. (1996) "Inverse Shape and Boundary Condition Problems and Optimization in Heat Conduction", Chapter 10 in *Advances in Numerical Heat Transfer*, Editors: W. J. Minkowycz and E. M. Sparrow, Taylor & Francis, pp. 324-367.

Foster, N. F. and Dulikravich, G. S. (January-February 1997) "Three-Dimensional Aerodynamic Shape Optimization Using Genetic and Gradient Search Algorithms", *AIAA Journal of Spacecraft and Rockets*, Vol. 34, No. 1, pp. 36-42.

Hafka, R. T. and Gurdal, Z. (1992) *Elements of Structural Optimization*, 3rd edition, Kluwer Academic Publishers, Boston, MA.

Han, J.-C., Zhang, Y. M., and Lee, C. P. (January 1994) "Influence of Surface Heating Condition on Local Heat Transfer in a Rotating Square Channel With Smooth Walls and Radial Outward Flow", *J. of Turbomachinery*, Vol. 116, pp. 149-158.

Han, Z.-X., Fang, R. and Liu, Z.-J. (1998) "2-D Flowfields Calculation with Multi-Unstructured Grids", *Journal of Aerospace Power*, in press.

Han, Z.-X. and Liu, Z.-J. (November 1997) "Numerical Calculation of 2-D Inviscid Flow-Fields on Unstructured Grids", *J. of Engineering Thermophysics*, Vol. 18, No. 6.

Holman, J. P. (1981) "Heat Transfer", Fifth Edition, McGraw Hill Book Company.

Kane, J. H. and Saigal, S. (1988) "Design Sensitivity Analysis of Solids Using BEM", *Journal of Engineering Mechanics*, ASCE, Vol. 114, No. 10, pp. 1703-1722.

Leonard, O., 1990, "Subsonic and Transonic Cascade Design", AGARD R-780, pp. 7-1:7-18.

Leonard, O. and Demeulenaere, A. (1997) "A Navier-Stokes Inverse Method Based On a Moving Blade Wall Strategy", ASME paper 97-GT-416, Orlando, FL.

Li, H. and Kassab, A. J. (June 1994) "A Coupled FVM/BEM Approach to Conjugate Heat Transfer in Turbine Blades", *AIAA Paper 94-1981*, 6th AIAA/ASME Joint Thermophysics and Heat Transfer Conference, Colorado Springs, CO.

Pirzadeh, S. (1993) "Structured Background Grids for Generation of Unstructured Grids by the Advancing-Front Method", *AIAA J.*, Vol. 31, No. 2, pp. 257-265.

Martin, T. J. and Dulikravich, G. S. (September 1997) "Aero-Thermal Analysis and Optimization of Internally Cooled Turbine Blades", *XIII International Symposium on Airbreathing Engines (XIII ISABE)*, Chattanooga, TN, ISABE 97-7165, Vol. 2, pp. 1232-1250.

Meric, R. A. (1995) "Differential and integral sensitivity formulations and shape optimization by BEM", *Engineering Analysis with Boundary Elements*, Vol. 15, pp. 181-188.

Mochizuki, S., Takamura, J., Yamawaki, S., and Yang, W. J. (1994) "Heat Transfer in Serpentine Flow Passages With Rotation", *Journal of Turbomachinery*, Vol. 116, pp. 133-140.

Stephens, M. A. and Shih, T. I.-P. (June 1997) "Computation of Compressible Flow and Heat Transfer in a Rotating Duct with Inclined Ribs and a 180-Degree Bend", ASME paper 97-GT-192, Orlando, FL.

White, F. M. (1988) *Heat and Mass Transfer*, Addison-Wesley Publishing Company, Reading, MA, pp. 272.

White, F. M. (1994) *Fluid Mechanics*, Third Edition, McGraw-Hill Book Company, New York.

Yamazaki, K., Sakamoto, J., Kitano, M. (June 1994) 'Three-Dimensional Shape Optimization Using the Boundary Element Method", *AIAA J.*, Vol. 32, No. 6.

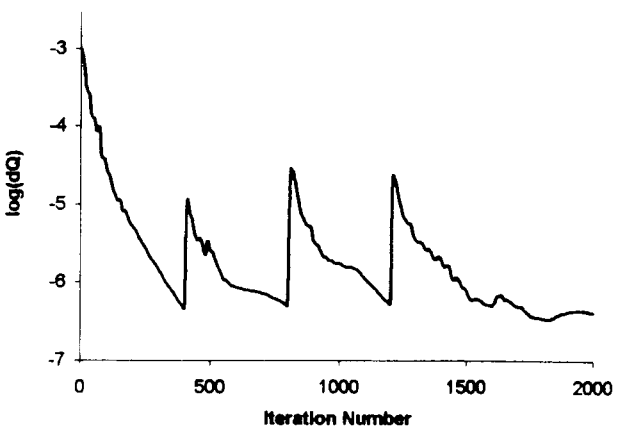

Fig. 1 Convergence history of the shape inverse design of symmetric airfoils in a non-lifting cascade.

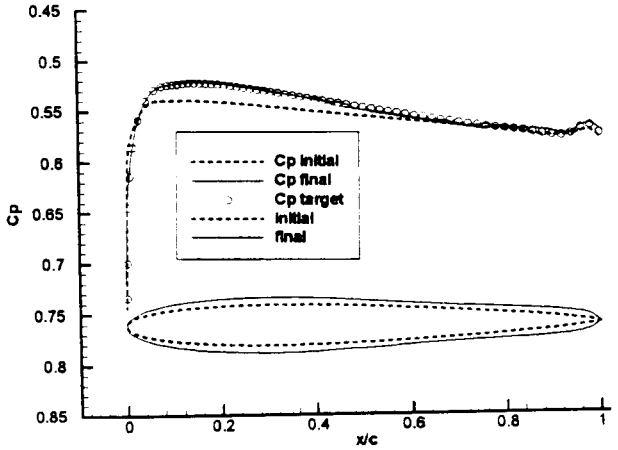

Fig. 2 Initial, target, and final isentropic surface Mach number distribution and initial and inversely designed symmetric airfoils in a non-lifting cascade.

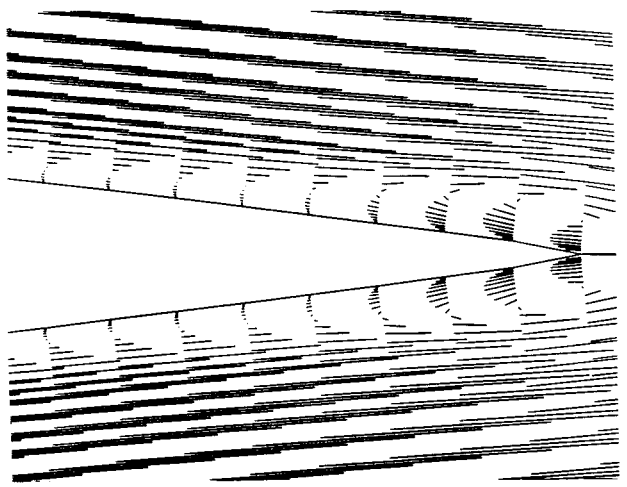

Fig. 3 Velocity field for the initial symmetric airfoils in a non-lifting cascade.

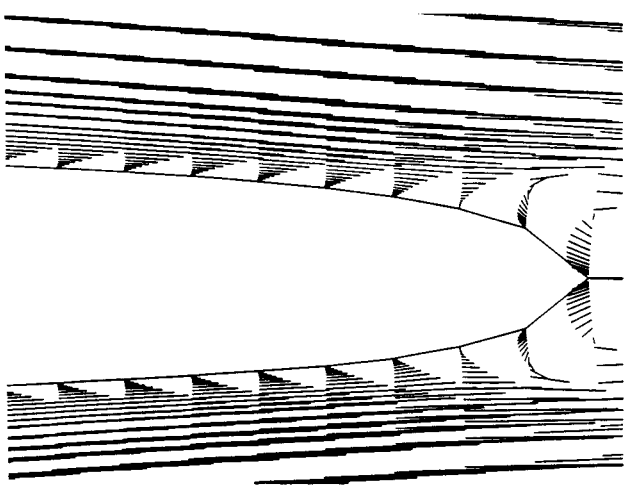

Fig. 4 Velocity field for the inversely designed symmetric airfoils in a non-lifting cascade.

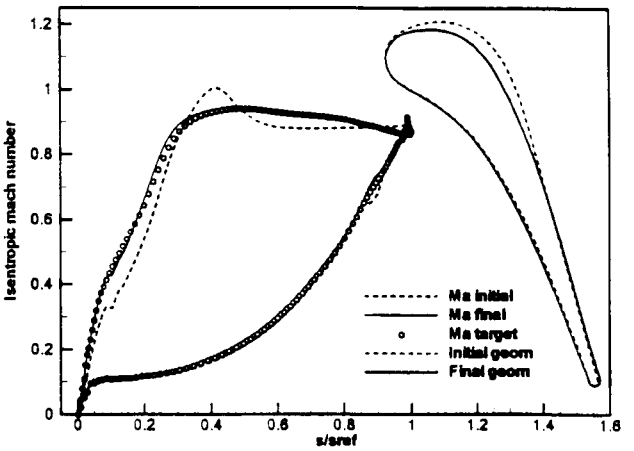

Fig. 5 Initial, target, and final isentropic surface Mach number distributions and initial and inversely designed high subsonic exit turbine cascade shapes.

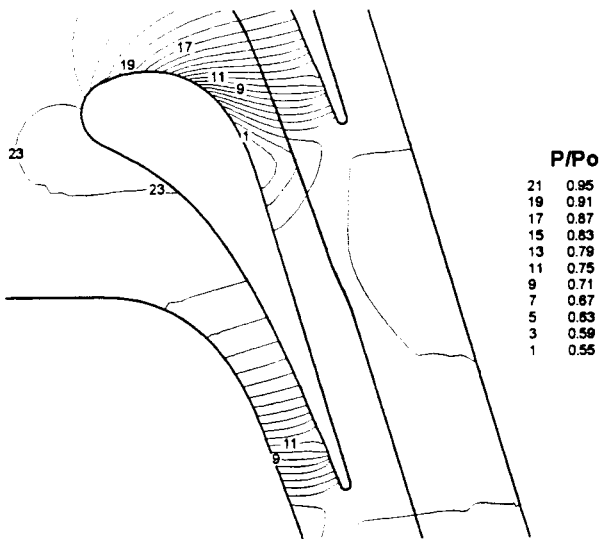

Fig. 6 Pressure field for an initial high subsonic exit turbine cascade obtained using Euler equations.

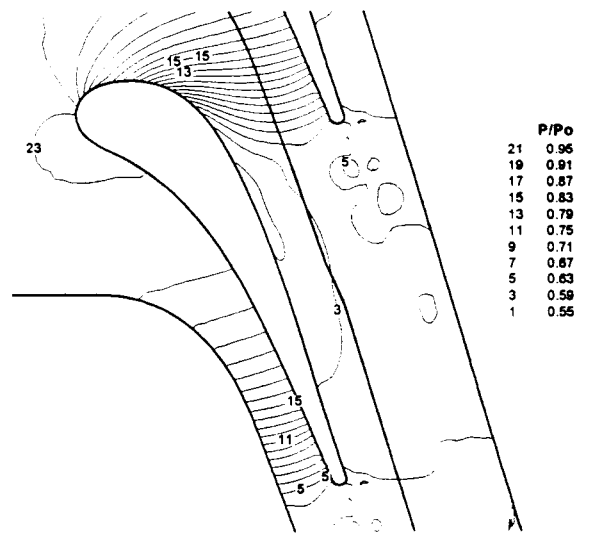

Fig. 7 Pressure field for the inversely designed high subsonic exit turbine cascade obtained using Euler equations.

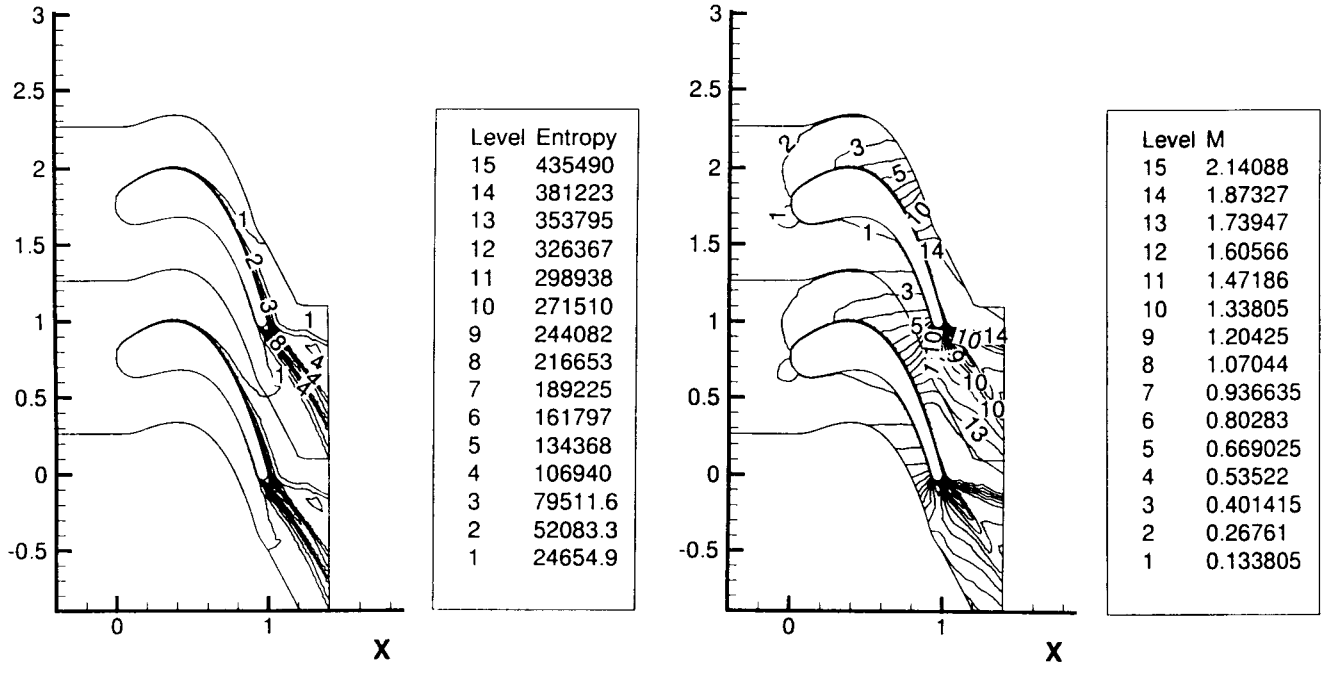

Fig. 8 Constant entropy and Mach number contours for the best airfoil after the first iteration cycle with a genetic optimizer and a Navier-Stokes flow-field analysis code.

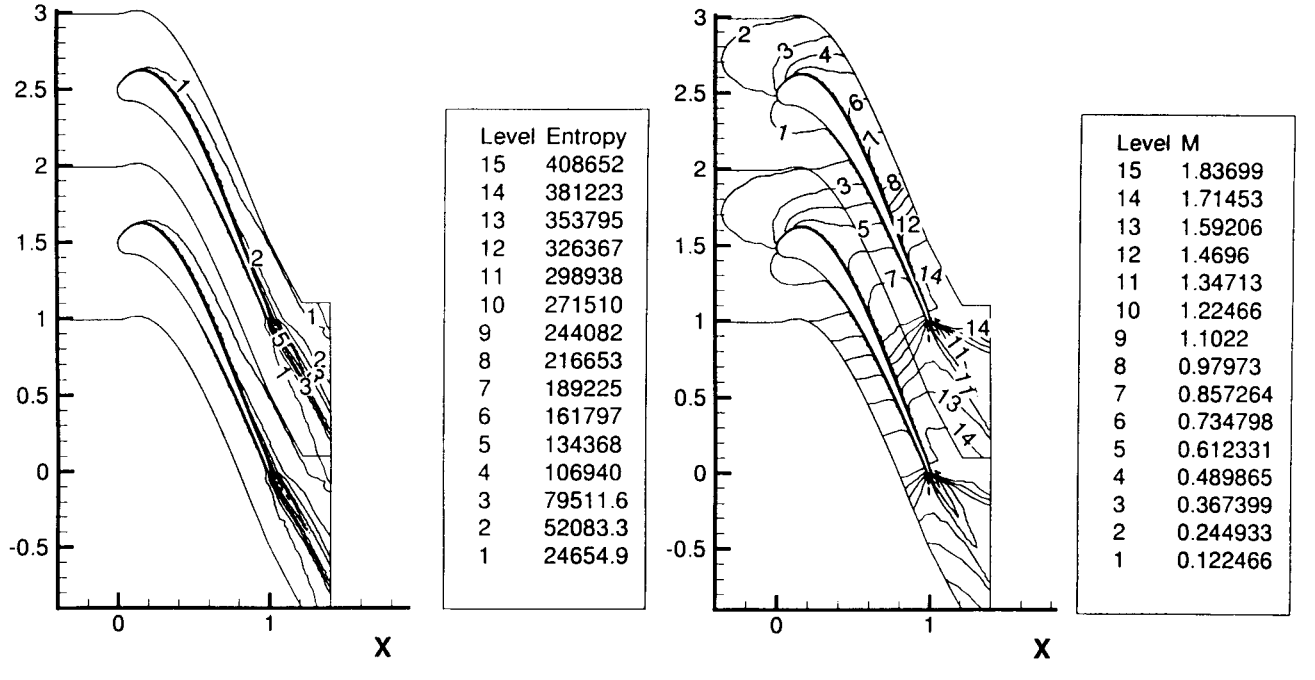

Fig. 9 Constant entropy and Mach number contours for the best airfoil after the tenth iteration cycle with a genetic optimizer and a Navier-Stokes flow-field analysis code.